Scanning Microscopy

Volume 1993
Number 7 *Physics of Generation and Detection of Signals Used for Microcharacterization*

Article 8

1993

Monte Carlo Simulation of X-Ray Spectra from Rh- and Cu-Targets Generated by kV-Electrons

K. Araki
Osaka University

Y. Kimura
Osaka University

R. Shimizu
Osaka University

Scanning Microscopy Supplement 7, 1993 (Pages 81-88) 0892-953X/93$5.00+.25
Scanning Microscopy International, Chicago (AMF O'Hare), IL 60666 USA

MONTE CARLO SIMULATION OF X-RAY SPECTRA FROM Rh- AND Cu-TARGETS GENERATED BY kV-ELECTRONS

K. Araki, Y. Kimura and R. Shimizu*

Department of Applied Physics, Faculty of Engineering, Osaka University,
Suita-shi, Yamada-oka 2-1, Osaka, 565, Japan

Abstract

Monte Carlo simulation is applied to calculate X-ray generation in thick targets under kV electron bombardment. As a preliminary examination, we adopted the simple model based on the uses of: (1)screened Rutherford scattering formula and Bethe's stopping power for describing elastic scattering and energy loss process of penetrating electrons, respectively, (2) Burhop's ionization-cross-section and Sommerfeld's Bremsstrahlung equation for generation of characteristic and continuous X-rays, respectively. In the Monte Carlo simulation, however, more practical expressions were used for convenience of calculation to describe generation of X-rays.

To see how precisely this Monte Carlo simulation describes X-ray spectrum generated in a thick target, we applied this approach to X-ray generation in Rh- and Cu-targets under bombardment by 50kV and 20kV electrons, respectively, to compare with experimental results.

This comparison has led to the conclusion that the present Monte Carlo simulation describes general tendency of X-ray spectra from the Rh- and Cu-targets with considerable success although the simulation tends to underestimate the X-rays intensity at long wave length.

Key Words: Monte Carlo, X-ray generation, Continuous X-rays, X-ray tube, X-ray Spectrum, Rh-target, Cu-target.

*Address for correspondence:
R. Shimizu
Department of Applied Physics,
Faculty of Engineering, Osaka University,
Suita-shi, Yamada-oka 2-1, Osaka, 565, Japan

Phone: 06-877-5111 ex.7841
Fax: 06-877-2900

Introduction

Recent marked progress of total refection fluorescence X-ray analysis (TRFX)[5] has been attracting renewed attention for X-ray spectra generated in thick targets bombardment with electrons with an energy of tens of kV. Designing a new type of X-ray tube requires the precise knowledge on the X-ray spectra generated under various boundary conditions. For this, theoretical calculations are needed to cover the deficiencies of basic experimental data since experimental investigations to determine the optimum operating conditions are time-consuming and laborious.

From a theoretical point of view, Monte Carlo calculation is probably the most useful approach, enabling X-ray spectra to be calculated under various boundary conditions. We have, therefore, attempted to develop a Monte Carlo simulation code, which allows us to describe a complicated scattering process of incident electrons associated with generation of continuous X-ray as well as characteristic X-ray in a target.

In the present work, we aimed at calculating the X-ray generation by the model as simple as possible in order to see whether or not it is worthwhile to develop a new, sophisticated Monte Carlo simulation code. Hence we decided to start from the simplest model, as a first trial, based on uses of: (1)Rutherford scattering formula and Bethe's stopping power equation to describe elastic scattering and energy loss of a penetrating electron, respectively[9], (2)Burhop's ionization cross-section[4] and Sommerfeld's equation[15] to describe generations of characteristic X-rays and continuous X-rays, respectively.

To verify this simple Monte Carlo approach, we performed Monte Carlo simulation of X-ray spectra generated from Rh-target by a 50 kV electron bombardment. The target has been widely used as an X-ray source for fluorescent X-ray analysis. The calculations were performed for two different boundary conditions, i.e., side-window type and

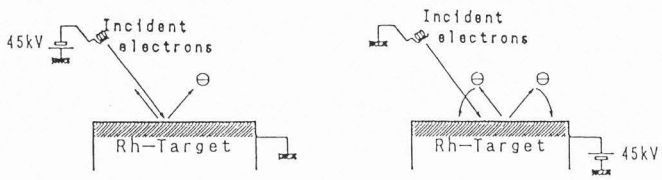

backscattered eletrons leave away from the target

backscattered electrons re-impinge on the target

Side window type End window type

Figure 1. Schematic diagrams of two different types of X-ray sources. (a)Side window type. (b)End window type.

end-window type, which are schematically illustrated in Fig. 1. In the case of end-window type, the backscattered electrons return to the target by the electric field to impinge on the target surface again. The efficiency of X-ray generation is, therefore, considerably improved.

Monte Carlo Simulation

Here we have aimed at describing the generation of X-ray by the model as simple as possible in order to get a feeling how this model should be improved to accommodate practical requirement for accurate theoretical prediction.

Electron trajectories

The trajectory of an incident electron in a target is described by the simplest modeling based on the use of the Rutherford scattering formula and Bethe's stopping power equation as follows:

(1) Elastic scattering

The screened Rutherford formula represented as[3]

$$\frac{d\sigma(\omega)}{d\Omega} = \frac{Z(Z+1)e^4}{4p^2v^2(1+2\gamma-\cos\omega)^2} \qquad (1)$$

with the screening parameter γ derived by Nigam et al.[13] as

$$\gamma = \frac{1}{4}(1.12\frac{\hbar\lambda_0}{p})^2 \qquad (2)$$

and

$$\lambda_0 = \frac{Z^{\frac{1}{3}}}{0.885a_0}, \qquad (3)$$

where a_0 is Bohr radius, Z atomic number, p the momentum of primary electrons and v the velocity of primary electrons.

(2) Inelastic scattering

Bethe's stopping power[1] in continuous slowing down approximation is used.

To take into account the relativistic effect, a first approximation to a relativistic stopping power formula derived by Bloch[4] is adopted in the present simulation because of its simplicity of the equation,

$$-\frac{dE}{dS} = \frac{4\pi e^4 nZ}{m_0v^2}\ln\frac{1.166m_0v^2}{2J(1-\beta^2)} \qquad (4)$$

$$J = 11.5Z \text{ [17]}, \qquad \beta = \sqrt{1-\frac{v}{c}} \qquad (5)$$

(c: velocity of light, n: atomic density).

The more exact formula for the relativistic stopping power which has been derived by Bethe[2] can be used for Eq. **(4)**, if needed.

Since the calculation procedures of this type of Monte Carlo simulation have quite often been reported[9], we don not repeat the explanation here.

X-ray generation

As an incident electron penetrates into a target, it generates continuous X-rays as well as characteristic X-rays. Here we assume that generation of these two types of X-rays is described by the Burhop expression for ionization cross-section[4] and Kirkpatrick & Wiedemann's representation[10] for characteristic X-rays and continuous X-rays, respectively, as follows.

Characteristic X-rays Ionization of shell-electrons is described by

$$Q = r\frac{\pi n_j e^4}{EE_j}b\ln\frac{4E}{B} \qquad (6)$$

where E_j is ionization energy of j-shell electrons and n_j number of j-shell electrons. The parameter b is given according to Green[7], by

$$b = 0.35\times1.73, \quad B = 4E_b \text{ (for K-ionization)} \qquad (7)$$

$$b = \frac{1}{4}(0.25)\times5.89, \quad B = 4E_b, \text{ (for } L_{III}\text{-ionization)} \qquad (8)$$

The correction factor

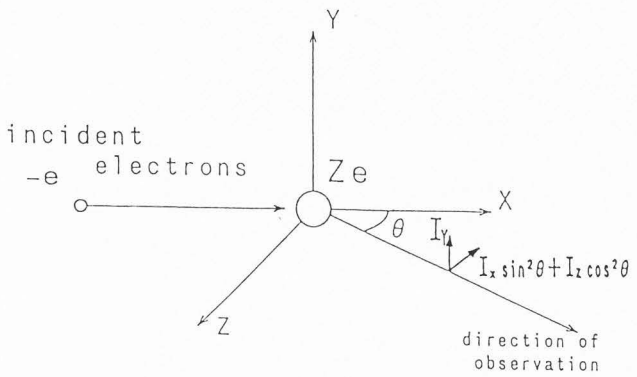

Figure 2. Generation of continuous X-rays(Bremsstrahlung) through the interaction between a fast electron and target atom.

$$r = \left(\frac{2+K_1}{2+K_2}\right)\left(\frac{1+K_2}{1+K_1}\right)^2\left[\frac{K_1 + K_2}{K_2+K_1\left(\frac{2+K_1}{2+K_2}\right)\frac{1}{(1+K_2)^2}}\right]^{\frac{3}{2}} \quad (9)$$

with $K_1=E_j/mc^2$ and $K_2=E/mc^2$ is to be inserted to Eq.(6) to take the relativistic effect into account[8]. Then, generation of characteristic X-rays is calculated simply by multiplying fluorescence yield, ω_p, to the ionization cross-section shown in Eq.(6).

Continuous X-rays We have used the expression derived by Kirkpatrick and Wiedemann[10] for the high energy region and that proposed by Statham[16] for the low energy region as follows:

The intensity of continuous X-rays to be observed at the direction, θ, measured from the axis of an incident electron (Fig. 2) is given by

$$\begin{aligned} I(\theta) &= I_x\sin^2\theta + I_y + I_z\cos^2\theta \\ &= I_x\sin_2\theta + I_y(1+\cos^2\theta) \\ &= I_x(1-\cos^2\theta) + I_y(1+\cos^2\theta) \end{aligned} \quad (10)$$

with relativistic correction factor

$$\left(1-\frac{v}{c}\cos\theta\right)^{-2} \quad (11)$$

According to Kirkpatrick and Wiedemann[10], I_x and $I_{y,z}$ are represented as follows:

$$I_x = \left\{0.252 + a\left(\frac{v}{v_0}-0.135\right) - b\left(\frac{v}{v_0}-0.135\right)^2\right\} \times 10^{-50} Z^2/V \quad (12)$$

$[\mathrm{erg\cdot cm^2/sterad\cdot Hz}]$

with v frequency of X-ray, v_0 frequency of de Broglie wave of electron and V acceleration voltage. Where

$$a = 1.47B - 0.507A - 0.833, \quad (13)$$

$$b = 1.70B - 1.09A - 0.627, \quad (14)$$

$$A = \exp(-0.223V/Z^2) - \exp(-57V/Z^2), \quad (15)$$

$$B = \exp(-0.0828V/Z^2) - \exp(-84.9V/Z^2). \quad (16)$$

With respect to $I_{y,z}$

$$I_{y,z} = \left\{-j + \frac{k}{v/v_0+h}\right\} \times 10^{-50}\ Z^2/V \quad (17)$$

$[\mathrm{erg\cdot cm^2/sterad\cdot Hz}]$

where

$$h = \frac{-0.214y_1+1.21y_2-y_3}{1.43y_1-2.43y_2+y_3}, \quad (18)$$

$$j = (1+2h)y_2 - 2(1+h)y_3, \quad (19)$$

$$k = (1+h)(y_3+j), \quad (20)$$

$$y_1 = 0.220(1 - 0.390\exp(-26.9V/Z^2)), \quad (21)$$

$$y_2 = 0.067 + 0.023/\{(V/Z^2)+0.75\}, \quad (22)$$

$$y_3 = -0.00259 + 0.00776/\{(V/Z^2)+0.116\}. \quad (23)$$

We have used the above equations (12) and (17) for the energy region, $V/Z^2 > 0.0604$.

For the low energy region, $V/Z^2 \le 0.0604$, we have used the expressions proposed by Statham[16],

$$I_x = e^x \qquad [10^{-50}\mathrm{erg\cdot cm^2/sterad\cdot Hz}] \quad (24)$$

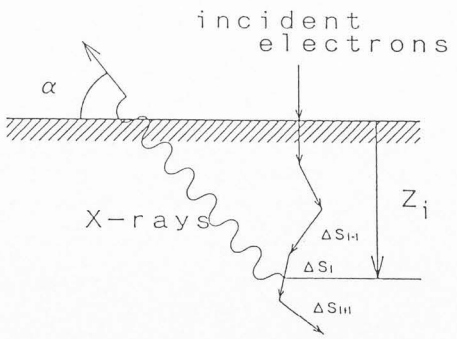

Figure 3. Schematic diagram of Monte Carlo calculations of both characteristic and continuous X-rays in a thick target.

$$I_y = e^y \qquad [10^{-50}\text{erg}\cdot\text{cm}^2/\text{sterad}\cdot\text{Hz}] \tag{25}$$

$$x = (-1.01904 + 0.146014R_f - 0.0501077R_f^2)\ln(V/Z^2) \\ -1.48311 + 0.947484R_f - 0.350014R_f^2, \tag{26}$$

$$y = (-0.882129 + 0.036693R_f - 0.339646R_f^2)\ln(V/Z^2) \\ -1.04088 + 1.86355R_f - 0.723068R_f^2, \tag{27}$$

$$R_f = v/v_0. \tag{28}$$

Simulation of X-ray Spectrum

First, we performed Monte Carlo simulation of electron trajectories and, then, calculated X-rays generated during the travel of the electron through the segment, ΔS_1, as seen in Fig. 3.

Since the intensity of the X-rays attenuates according to the exponential decay law before coming out from the target, the X-ray spectrum was obtained from the equations as follows:

$$I_b = \sum \frac{1}{4\pi}\left\{nQ(E_i,E_b)\omega_b \exp\left(-\frac{n\sigma_{ab}(\lambda_b)Z_i}{\sin\alpha}\right)\right\}\Delta S_i \tag{29}$$

for characteristic X-rays and

$$I_b = \sum \left\{nI(E_i,\lambda,\theta_i)\exp\left(-\frac{n\sigma_{ab}(\lambda_b)Z_i}{\sin\alpha}\right)\right\}\Delta S_i \tag{30}$$

for continuous X-rays.

Boundary condition

As a boundary for the end-window type we simply assumed that those backscattered electrons which leave the target surface with energy E′ at ejection angle α are impinging on the target surface with energy E′ at angle of incidence α, as schematically illustrated in Fig. 4. For the side-window type, we assumed that the backscattered electrons do not contribute any more to X-ray generation.

The cut-off energy for simulation of electron trajectories is set at either 5 keV or E = J / 1.166.

Absorption

Absorption of X-rays in a Rh target and a Be-window are calculated according to the following equation[12],

$$I = I_0\exp(-\mu_{ab}d) = I_0\exp(-n\sigma_{ab}d) \tag{31}$$

where

$$\sigma_{ab} = \sigma_{Rh}(x) = \sum \exp(a_{j0}+a_{j1}x+a_{j2}x^2+a_{j3}x^3)\ [\text{cm}^2] \tag{32}$$

for Rh and

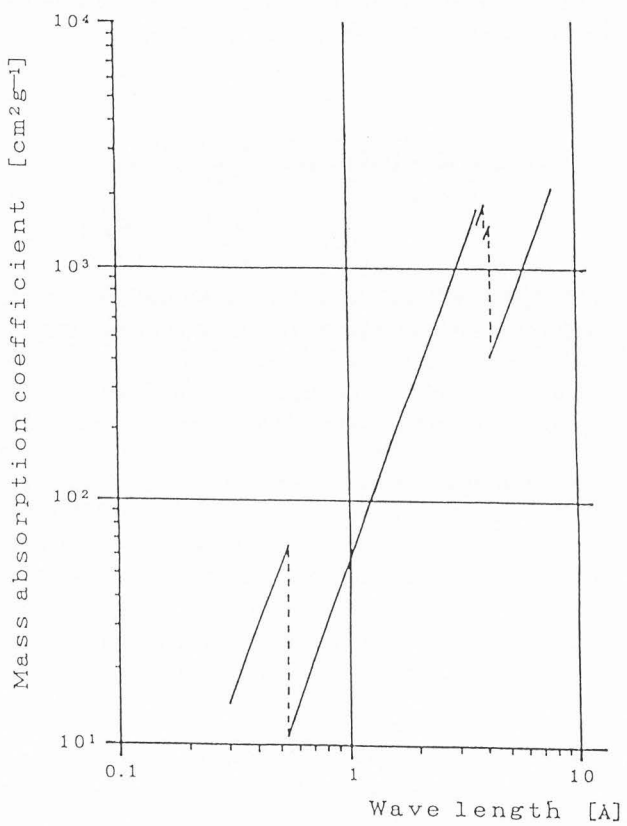

Figure 4. Mass-absorption coefficient for Rh- target calculated from Eq.(31).

Table 1. Parameters for describing absorption of X-ray of various wave lengths in Be-target

j	b_{j0}	b_{j1}	b_{j2}	b_{j3}
1 Thomson scattering	2.0086	-0.046192	-0.337018	0.0186939
2 Compton scattering	-0.690079	0.946448	-0.171142	0.00651413
3 Photoelectric absorption	9.04511	-2.83487	-0.210021	0.0229526

$$\sigma_{ab} = \sigma_{Be}(x) = \sum \exp(b_{j0}+b_{j1}x+b_{j2}x^2+b_{j3}x^3) \quad [cm^2] \quad (33)$$

for Be with x = ln E where E is photon energy, hc/λ.

The parameters in Eqs. **(32)** and **(33)** are listed in Tables 1 and 2, respectively, and the mass absorption coefficient of Rh assessed from Eq. **(32)** is depicted as a function of wave length in Fig. 5.

Results and Discussion

Fig. 6 shows the calculated X-ray spectra for the end-window type. The experimental result obtained for the end-window type is also depicted for comparison. All these spectra are normalized by taking the height of K-absorption edges as unity.

With respect to the general qualitative tendency, the present Monte Carlo simulation describes the experiment with considerable success even though very simple model is adopted. From a quantitative point of view, however, it is obvious that the simulation tends to overestimate the X-ray intensity in the short wave length region and to underestimate it for longer wave lengths.

Another examination was done for the intensity ratio of characteristic X-rays to continuous X-rays. The comparison with experiment is shown in Table 3. The simulation underestimates the intensity ratio the over all wavelengths. Hence, both the results for end-window type and side-window type suggest that the present calculation either underestimates the generation of continuous X-rays or overestimates the intensity of characteristic X-rays.

Since the returning of backscattering electrons plays an important role in the case of end-window type, further improvements of modelling should be made as follows:

(1) The boundary condition for backscattered

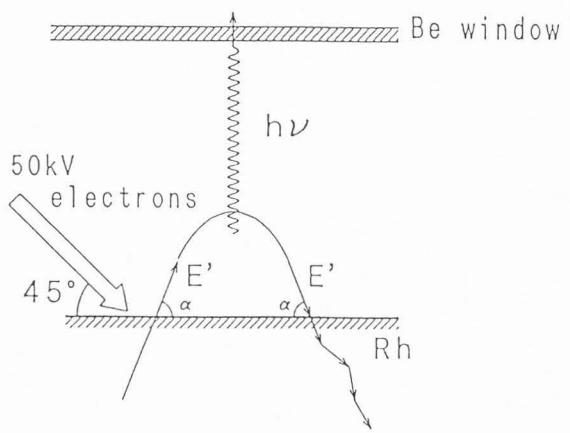

Figure 5. Simple model of the end window type X-ray source in practical use for Monte Carlo calculation.

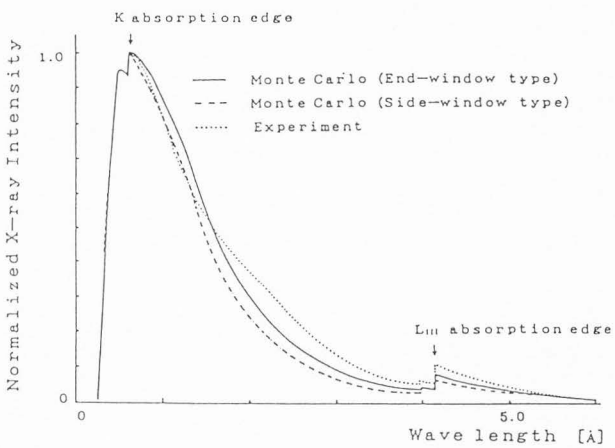

Figure 6. Comparison of the X-ray spectrum form Rh-target between experimental[11] and Monte Carlo calculation results under the conditions; primary beam energy 50keV, angle of incidence 45°, take off angle of X-rays 90° (normal to the target surface) thickness of Be window 0.127 mm.

Table 2. Parameters for describing absorption of X-ray of various wave lengths in Rh-target

j	a_{j0}	a_{j1}	a_{j2}	a_{j3}
1 Thomson scattering	6.97547	0.346394	-0.367794	0.0187885
2 Compton scattering	-0.160399	1.64861	-0.250238	0.00893818
3 M absorption edge	14.0312	-2.61303	0.	0.
4 K absorption edge	14.2042	-0.377628	-0.491746	0.0314037
5 L_I absorption edge	12.5344	-1.27106	-0.214684	0.00634304
6 L_{II} absorption edge	14.2564	-2.17111	-0.246238	0.014971
7 L_{III} absorption edge	14.6945	-2.03357	-0.29045	0.0163374

Table 3. Comparison of intensity ratio of characteristic X-rays to continuous X-rays between Monte Carlo calculation and experiment

Radiation	Monte Carlo		Experiment
	Window type		
	[End]	[Side]	[End]
Rh Kα	0.146	0.163	0.258
Rh Kβ	0.0307	0.0327	0.046
Rh Lα	6.887	7.346	7.578
Rh Lβ	2.113	2.261	2.435

electrons should be more realistic one, simulating the experimental condition more accurately.

(2) The screened Rutherford cross-section should be replaced by Mott cross-section, since the screened Rutherford is a poor approximation for heavy elements and high energy region[14].

Another application of the present Monte Carlo approach to the X-ray spectrum generated from Cu-target is shown in Fig.7.

The calculation was made for the conditions; primary electrons of 20keV, angle of incidence α= 0°(normal to the target surface), detector angle of X-rays 52° and Si-detector with Be-window of 15 microns thick. The measurement was done, first, by setting the target surface roughly normal to the primary electron beam. Then, the measurements were repeated by tilting the target at ±20° against the detector to see how the detector angle influences the X-ray spectrum, particularly, in lower energy region. The results were shown for α=0° and 20° in Fig.7 to compare with the calculation. It is clearly seen that the calculated spectrum is in between the two measured spectra but much closer to that for α=20°. This result is another confirmation of the applicability of the present Monte Carlo modeling for electron probe microanalysis.

With respect to the Sommerfeld theory of continuous X-rays generation, a simple examination was also done for angular distribution of continuous X-rays generated in a thin Al-film of 0.6 μm thick under 31 kV electron bombardment by comparing the theory with the experiment of Kulenkampff[11]. The results are shown in Fig.8. For longer wavelengths, ~0.73Å, the calculation describes the experiment quite well while the agreement between the calculated and experimental results is not so good for shorter wave lengths, ~0.53Å and ~0.43Å. This sort of examination should be done for the present study on Rh- and

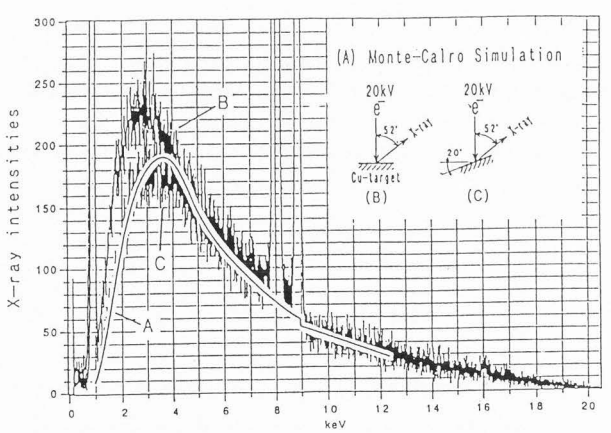

Figure 7. Comparison of X-ray spectrum from Cu-target between Monte Carlo calculation and experiment. The calculation(A) was done for the experimental conditions; primary energy of electron beam 20keV, angle of incidence 90° and detection angle of X-rays 38°. The two spectra were measured under the same conditions but angles of incidence, α=0°(B) and α=20°(C).

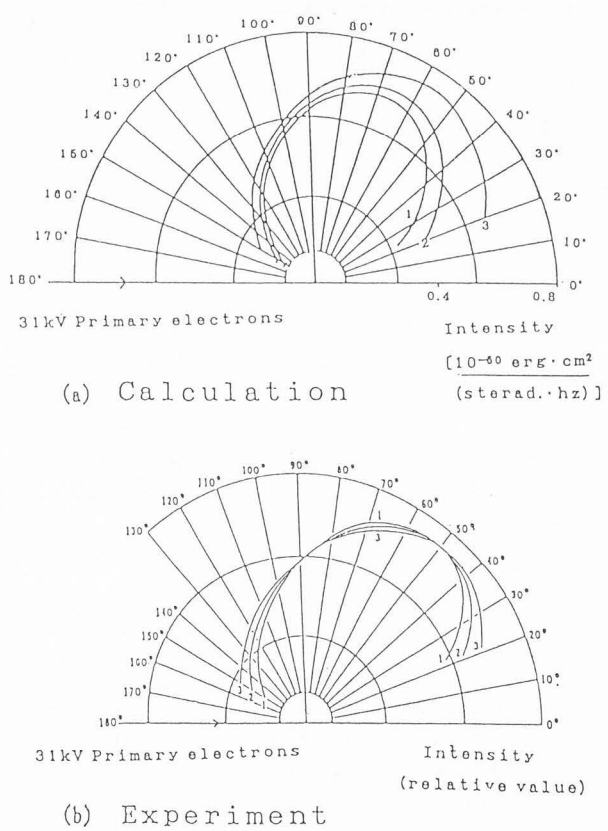

Figure 8. Comparison of Angular distribution of continuous X-rays generated in an Al-thin film of 0.6 micron thick under 31 kV electron bombardment between experimental[11] and Monte Carlo calculation results. 1, λ~0.43Å; 2, λ~0.53Å; 3, λ~0.73Å.

Cu-targets. For this, a systematic experimental investigation on angular distribution of continuous X-rays generated in thin films of Rh and Cu is most helpful. Thin film analysis by analytical electron microscopy[6] for different primary energies will also provide another useful examination of the Sommerfeld theory.

In conclusion, even though the simplest model was adopted for the simulation, the present Monte Carlo simulation describes the general tendency of the X-ray spectra from Rh- and Cu-targets with considerable success. This result is encourageous enough, suggesting that further improvements of the present model leads to better agreement with experiment and provides useful theoretical predictions of X-ray spectra generated under various conditions of practical importance.

Acknowledgements

The authors are very grateful to the staff members of RIGAKU Corp., particularly, to Mr. Y. Kataoka for providing the experimental data on the X-rays spectrum from Rh-target and helpful advice for Monte Carlo simulation. Thanks are also due to Mr. K. Obori, HORIBA Ltd., for the measurement of X-rays spectra from Cu-target and for stimulating discussion on the experimental condition.

References

[1]Bethe HA (1930), Zur Theorie des Durchgangs schneller Korpulskularstrahlen der Materie (For theories on passage of fast particle through matter), Ann. d. Phys. **5**, 325-400.

[2]Bethe HA (1933), Quantenmechanik der Ein- und Zwei-Elektronenprobleme (Quantum mechanics of one- and two-electrons problem), in Handbuch der Physik, Ed. S.Flügge (Springer, Berlin, 1933) vol. 24, 273-560.

[3]Bethe HA (1953), Moliere's Theory of Multiple Scattering, Phys. Rev. **89**, 1256-1266.

[4]Birkhoff RD (1958), The Passage of Fast Electron Through Matter, in Handbuch der Physik, Ed. S. Flügge (Springer, Berlin, 1958) vol. 34, 53-138.

[5]Eichinger P, Rath HJ and Schwenke H (1989), Application of Total Reflection X-ray Fluorescence Analysis for Metallic Trace Impurities on Silicon Wafer Surface, Semiconductor Fabrication: Technology and Metrology, ASTM STP 990 Ed. C.Gupta (American Society for Testing and Materials, 1989) 305-313.

[6]Goldstein JI (1979), Principles of thin film X-ray microanalysis, in Introduction to Analytical Electron Microscopy, Eds. Hren JJ, Goldstein JI and Joy DC (Plenum, New York, 1979) 83-120.

[7]Green M (1962), The Efficiency of Production of characteristic X-ray Radiation, Ph. D. Thesis, University of Cambridge (1962).

[8]Gryzinski M (1965) Two-Particle collision I, II, III, Phys. Rev. **138** A 305-358.

[9]Heinrich KFJ, Newbury DE and Yakowitz H (1976), Use of Monte Carlo Calculation in Electron Probe Microanalysis and Scanning Electron Microscopy, (NBS-Special Publication 460) (National Bureau of Standard, Washington D.C.) 61-95.

[10]Kirkpatrick P and Wiedemann L (1945), Theoretical Continuous X-ray Energy and Polarization, Phys. Rev. **67**, 321-339.

[11]Kulenkampff H (1928), Untersuchungen der Kontinuierlichen Röntgenstrahlung dünner Aluminiumfolien (Study on continuous X-rays from thin aluminum films), Ann. d. Phys. **87**, 597-637.

[12]McMaster WH, Kerr Del Graude N, Mallett JH and Hubbell JH (1969), Compilation of X-ray Cross Sections, Documents UCRL 50174, National Technical Information Source, National Bureau of Standards (Springfield, Va, 1969).

[13]Nigam BP, Sundersen MK and Ta-Yon Wu (1959), Theory of multiple scattering: second Born approximation and corrections to Moliere's work, Phys. Rev. **115**, 491-502.

[14]Shimizu R, Ichimura S and Aratama M (1979), Application of Monte Carlo calculation technique to quantitative analyses by Auger electron Spectroscopy, in Microprobe Analysis, Ed. D.L. Newbury (San Francisco Press, San Francisco, 1979) 30-34.

[15]Sommerfeld A (1931), Über die Beugung und Bremsung der Elektronen (On deflection and deceleration of electrons), Ann. d. Phys. 11, 17-330.

[16]Statham PJ (1976), The generation, Absorption of Thick-target Bremsstrahlung and Implications for Quantitative Energy Dispersive Analysis, X-Ray Spectrometry **5**, 154-168.

[17]Yoshikawa H, Takeguchi M and Shimizu R (1991), Calculations of Electric fields by Space Charge Method for Designing TFE Gun, Tchnol. Repts. Osaka Univ. **41**, No.2032(1991)17-23.

Discussion with Reviewers

G. Love: The emitted X-ray intensities will clearly be influenced by the amount of absorption experienced in the target and the beryllium detector window, particularly at long X-ray wavelengths. The equation used to calculate the mass absorption coefficient does not appear to be referenced, and do the authors have any knowledge of its accuracy for wavelengths greater than, say, 3Å where its value appears to approach 1000 cm^2gm^{-1}?

Authors: The expression of the equations **(32)&(33)** are to be corrected. The absorption coefficient of Be for ~3Å calculated from eq. **(33)** (which is corrected) agrees with the experimental value within 5% of error. The reference is also quoted.

Thank you very much for drawing our attention to the mistakes of the equations in the manuscript.

G. Love: In Table 3 where experimental characteristic to continuum X-ray intensities are compared with Monte Carlo data, there is no only one set of experimental results listed. Does the experimental ratio not change depending on whether or not the target is positively biased?

Authors: Yes, the ratio does change depending on whether or not the target is positively biased.

G. Love: the authors indicate in a little more detail how they would make the boundary condition for backscattered electrons more realistic in the case of an end window type source?

Authors: The trajectories of backscattered electrons in a given geometry of the end-window type X-ray source can be simulated by the simulation code which we had developed[17]. The detail of the geometry of the end-window type, however, has not been allowed to be presented as yet.

G. Love: It would be helpful if further information was given on how accurate the simulation needed to be for this type of application. Clearly, the experimental and theoretical results do not match, but what level of fit would be acceptable?

Authors: We are expecting that the present Monte Carlo calculation can describe EDX-spectra (e.g., shown in Fig.7) with considerable success provided that more accurate differential cross-sections for elastic scattering is used. Although the theoretical expressions for individual process, e.g., elastic and inelastic scattering, angular distribution of continuous X-rays generated in thin film (see Fig.8), etc, are not absolutely accurate, we believe the net characteristic such as X-ray generation can be described in thick targets by the present Monte Carlo simulation with appropriate modification.

K. Murata: Could you give the validity of the absolute X-ray intensity of your calculation?

Authors: The comparison of absolute X-ray intensity between the Monte Carlo simulation and experiment would be the next subject, for verifying the theoretical model. For this, an EDX-spectrum may be an appropriate target though some corrections for the signal detecting system are needed.

K. Murata: Could you comment on the physical reason why the side-window type is larger than that with the end-window type?

Authors: Simply speaking, the intensity of continuous X-rays from a thin film, for instance, is proportional to 1/E while that of characteristic X-rays is proportional to (1/E)lnE, where E is the energy of a penetrating electron. Hence, the intensity ratio of characteristic X-rays is coarsely proportional to lnE. This suggests that a larger contribution of low energy electrons [the case of end-window type] tends to decrease the value of the ratio.